RMIT UNIVERSITY

bushfire&natural HAZARDSCRC

BLACK SUMMER 2019–20 RESEARCH
bnhcrc.com.au

KANGAROO ISLAND BLACK SUMMER 2019-20 FIRE RECONSTRUCTION

Simon Ramsey, Karin Reinke, Nur Trihantoro, Simon Jones & Chermelle Engel

RMIT University & Bushfire and Natural Hazards CRC

Version	Release history	Date
1.0	Initial release of document	26/07/2021

Australian Government
Department of Industry, Science, Energy and Resources

AusIndustry
Cooperative Research Centres Program

Publisher:
Bushfire and Natural Hazards CRC

July 2021

Citation: Ramsey S, Reinke K, Trihantoro N, Jones S & Engel C (2021) Kangaroo Island Black Summer fire reconstruction, Bushfire and Natural Hazards CRC, Melbourne.

Cover: Kangaroo Island fire. Source: Rob Hartill, South Australian Country Fire Service Promotions Unit

TABLE OF CONTENTS

ACKNOWLEDGEMENTS

This research was part of the Bushfire and Natural Hazards Cooperative Research Centre's Black Summer research program, funded by the Australian Government and the CRC to investigate key issues from the 2019-20 bushfire season.

INTRODUCTION

In the 2019-20 summer, wildfire affected an area of around 200,000 hectares on Kangaroo Island, South Australia, in what has become known as the Black Summer, with significant ongoing social, economic and environmental impacts.

The Advanced Himawari Imager (AHI) onboard the geostationary satellite Himawari-8 provides infrared imagery at 2km spatial resolution at nadir in 10-minute intervals. This allows wildfires to be detected and monitored in quasi-real time using the Biogeographical Region and Individual Geostationary HHMMSS Threshold (BRIGHT) algorithm (Engel, Jones and Reinke, 2020), developed in partnership between the Royal Melbourne Institute of Technology (RMIT) and the Bushfire and Natural Hazard CRC. This report outlines the methods used to verify hotspots detected by the BRIGHT algorithm and reconstruct the Black Summer fires using spatio-temporal clustering.

RESEARCH APPROACH

DATA AND SOFTWARE

The data set used in this assessment consisted of 20,371 detections of active fire over Kangaroo Island by the BRIGHT algorithm for the period from December 1st, 2019 until February 1st, 2020. Detections were compared to NASA's MCD14DL active fire product (Giglio, 2016) and MCD64A1 Collection 6 burned area product (Giglio, Louis *et al.*, 2015) for the Moderate Resolution Imaging Spectroradiometer (MODIS). The MODIS system, on board the Terra and Aqua satellites, provides two day and two night observations of fire activity daily. The burned area intercomparison against MCD64 was performed in ArcGIS Pro.

Commission and omission errors were calculated against MCD14DL as outlined in the manuscript by Engel, Jones and Reinke (2021).

To flag BRIGHT hotspots which were deemed to be false positives (errors of commission),and remove them from the data to be used in the reconstruction, the BRIGHT data was compared to MCD64A1 to assess whether BRIGHT detections were spatially and temporally coincident with burn scars mapped by MODIS. BRIGHT hotspots, which are data points representing the centroid of an AHI pixel, were first buffered at 1.8km radius (Appendix A) to ensure inclusivity of all intersecting MODIS pixels in the analysis. The output was then compared to MCD64A1 using the method outlined in Figure 1. From the MCD64 data, the first evidence of fire activity on Kangaroo Island was mapped on December 9th, 2019 and ended on January 16th, 2020.

METHOD (COMPARISON OF BRIGHT HOTSPOTS AGAINST MODIS FIRE PRODUCTS)

Commission errors were calculated by a spatial intercomparison with the MODIS burned area product MCD64A1, and assigned a binary flag based on spatial agreement (Figure 1).

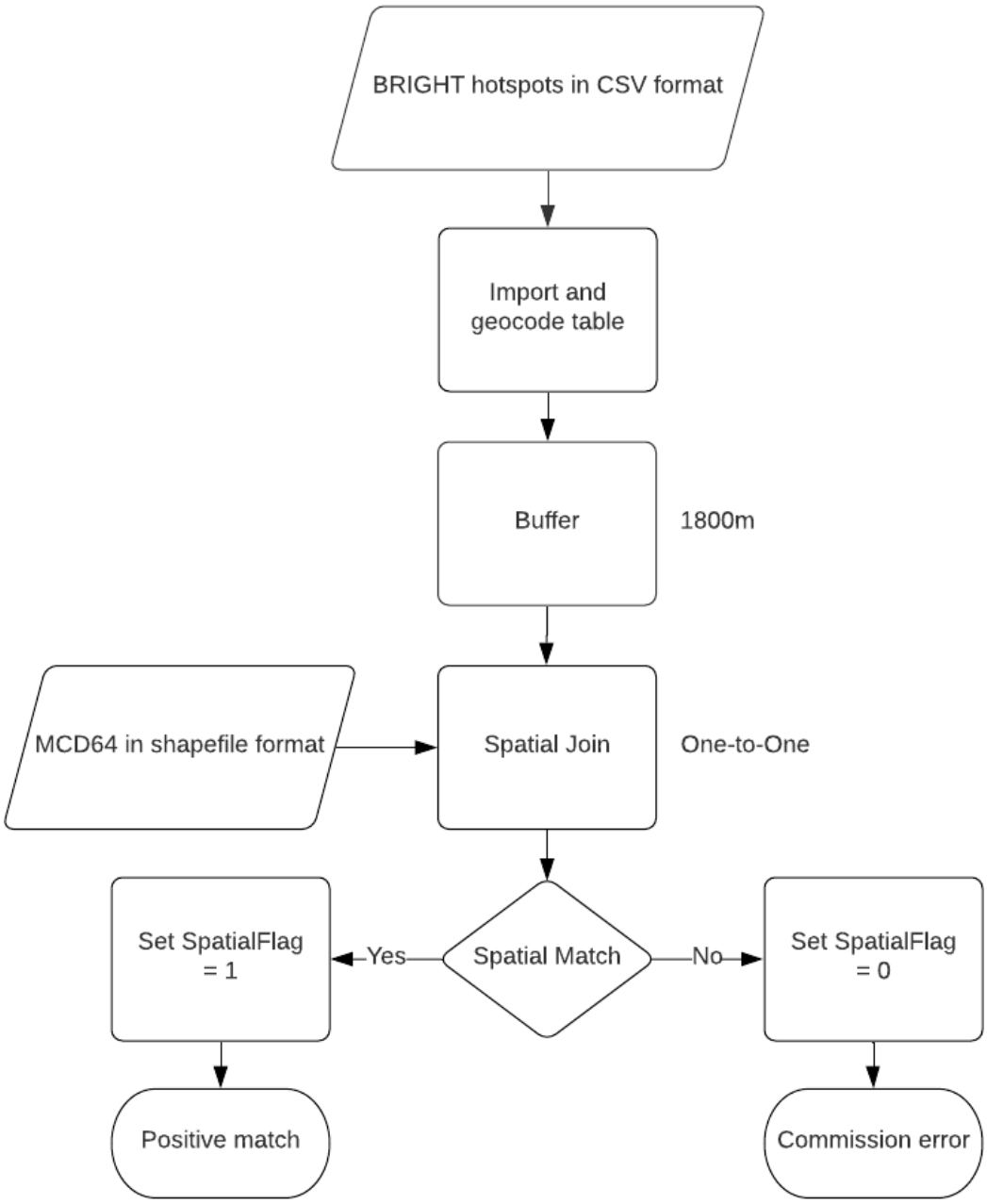

FIGURE 1. ARCGIS PRO WORKFLOW FOR CALCULATING COMMISSION ERRORS AND FLAGGING SPATIAL DISAGREEMENTS BETWEEN THE BRIGHT ALGORITHM AND MCD64.

Omission errors were calculated by determining the area without spatial overlap between the BRIGHT detections and MCD64A1 as a percentage of total area burned. This was performed using the workflow outlined in Figure 2. The results from these analyses are reported in Table 2.

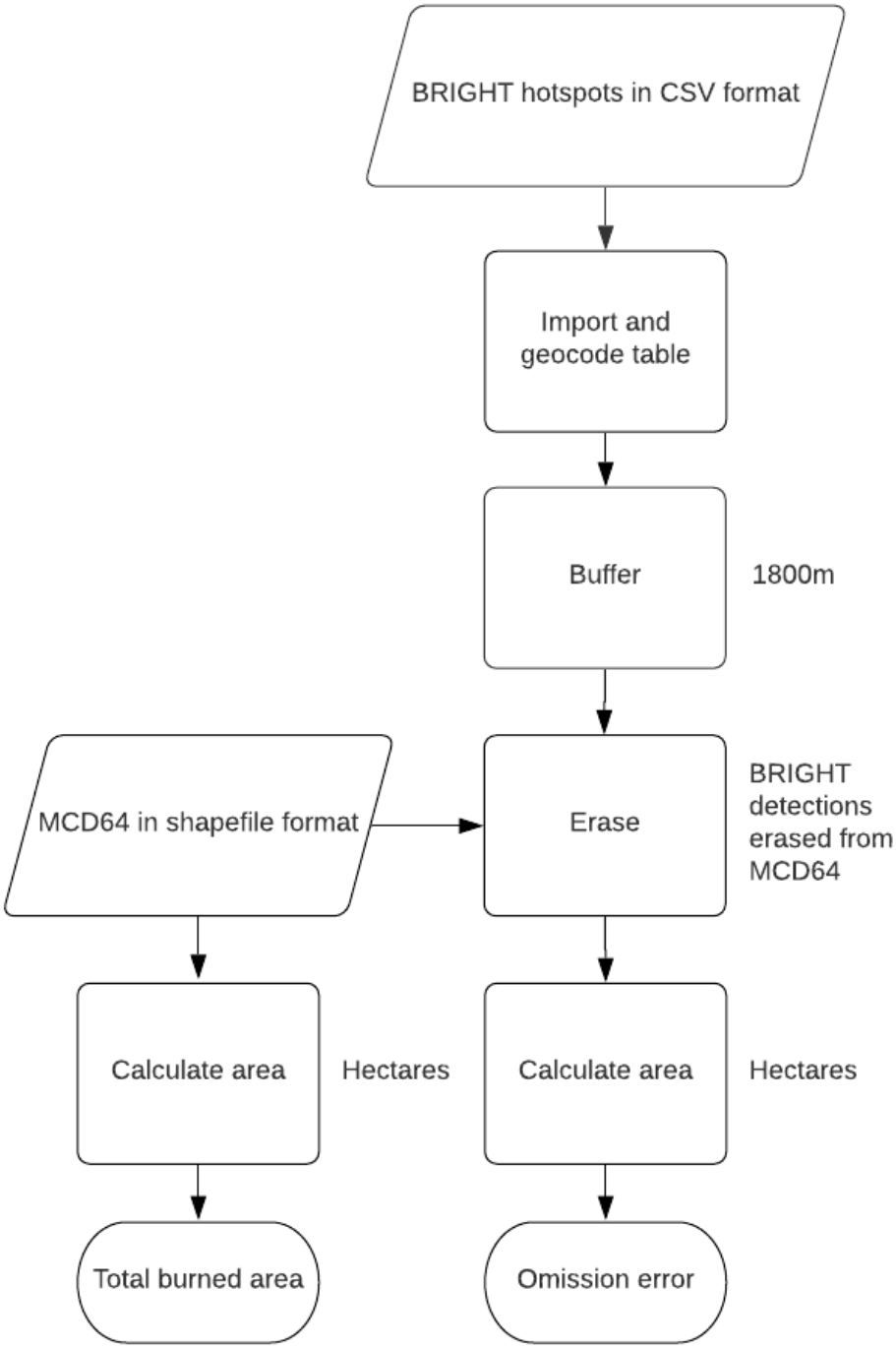

FIGURE 2. ARCGIS PRO WORKFLOW FOR CALCULATING OMISSION ERRORS AS A PERCENTAGE OF AREA WITH NO SPATIAL OVERLAP BETWEEN BRIGHT HOTSPOTS AND MCD64.

FIGURE 3. REGIONS OF BRIGHT OMISSION IN THE MCD64 DATA (YELLOW). BRIGHT HOTSPOTS IN AGREEMENT IN BLUE. BRIGHT HOTSPOT COMMISSION IN RED.

Between January 2nd and January 5th, 2020, a large data gap* is present in the BRIGHT active fire data (Figure 3). Further investigation showed this was the result of large plumes of smoke obscuring the Middle Infrared (MIR) signal which affected both the BRIGHT algorithm and the MODIS active fire product (Figure 4). (*The presence of data gaps can affect the experimental data products and attributes prepared in this work; that is, the identification of superclusters and respective seed points. These are noted throughout the report and in the associated metadata tables.

FIGURE 4. MODIS CORRECTED REFLECTANCE (TRUE COLOUR) IMAGERY FROM JANUARY 2ND, 2020. THICK SMOKE OBSCURED THE INFARED SIGNAL AFFECTING BOTH MODIS AND AHI ACTIVE FIRE PRODUCTS. THE LARGEST DATA GAP IS WITHIN THE RED ELLIPSE. SOURCE: EOSDIS WORLDVIEW.

AGREEMENT BETWEEN HOTSPOTS

AGREEMENT WITH MCD14DL ACTIVE FIRE

BRIGHT hotspots were initially assessed for agreement with the MODIS active fire product (MCD14DL). The assessments were conducted for all BRIGHT hotspots detected without any data filtering. Assessments were constrained to check presence/absence of BRIGHT hotspots that were temporally and spatially coincident with the comparison MODIS product. Day and night readings by MODIS were combined in this assessment. The process for this comparison is described in Engel, Jones and Reinke (2021).

AREA	KANGAROO ISLAND
Number of BRIGHT hotspots in the MODIS reconstructed swaths	293
Number of BRIGHT hotspots detected within 1 pixel of a MODIS hotspot	267
Commission error (possible missed detections) for BRIGHT hotspots	*8.87%*
Number of MODIS hotspots (collated on the AHI grid)	290
Number of MODIS hotspots (collated on the AHI grid) detected within 1 pixel of a BRIGHT hotspot	228
Omission error (possible false detections) for BRIGHT hotspots	*21.38%*

TABLE 1. AHI BRIGHT ALGORITHM AND MODIS MCD14DL ACTIVE FIRE PRODUCT INTERCOMPARISON FOR KANGAROO ISLAND AND SOUTH-EASTERN AUSTRALIA FOR DECEMBER 2019 – JANUARY 2020.

VERIFICATION AGAINST MCD64A1 BURNED AREA

MCD64A1 is a widely regarded burned area mapping algorithm created from imagery collected by the MODIS system producing a daily global product sensitive to fire activity resulting in changes to landcover and surface reflectance. The burn scars mapped by MCD64A1 were used to identify commission errors; where a BRIGHT hotspot had been detected without the presence of a spatially coincident burn scar mapped by MODIS, and omission errors; the area covered by the MCD64A1 burned area product which had no spatial overlap with BRIGHT hotspots Table 2.

	TOTAL	SPATIAL MATCHES	AGREEMENT	ERROR
Commission (by count of BRIGHT hotspots)	*20,371*	*20,227*	*99.29%*	*0.71%*
Omission (by area of MCD64 in ha)	*198,618*	*176,435*	*88.83%*	*11.17%*

TABLE 2. RESULTS FROM INTERCOMPARISON OF BRIGHT WITH MCD64.

Omission was significantly affected by smoke obscuring the thermal signal. This resulted in a data gap in the BRIGHT data shown in Figures 3 and 4, explaining the relative increase in the total omission error compared to the burned area product.

SPATIO-TEMPORAL CLUSTERING

FIXED TIMES CLUSTERING METHOD

The overall clustering method was based on the spatio-temporal clustering process by Lizundia-Loiola *et al.* (2020). Figure 5 below shows the process of creating the fixed times Himawari-8 hotspot clusters dataset. After separating the cleaned hotspots data based on their epoch, a 1.8 km buffer is applied. For each 2-hour time window, the clusters were created by merging all overlapping buffered hotspots.

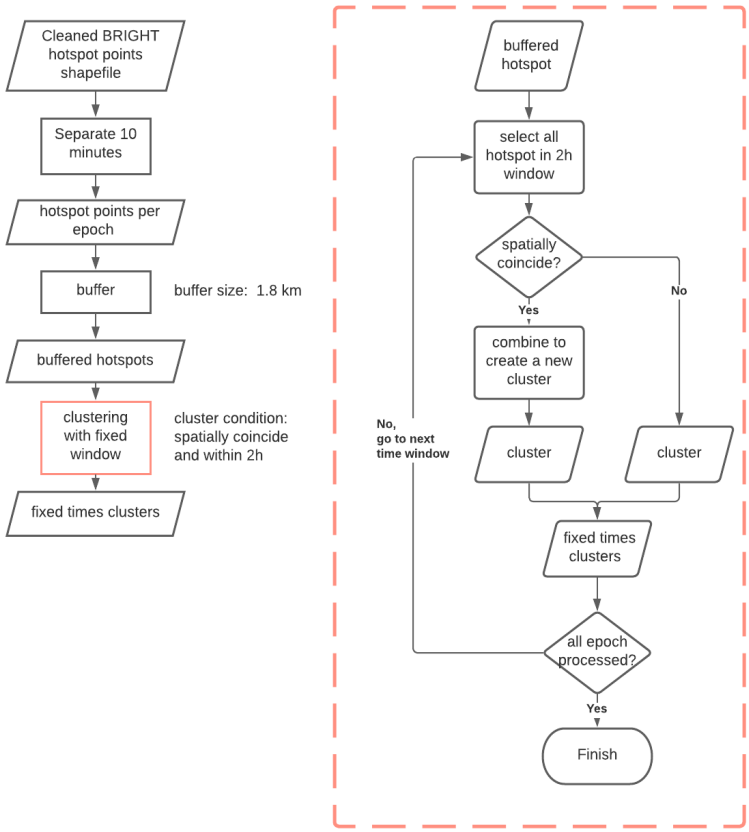

FIGURE 5. FIXED TIMES HOTSPOTS CLUSTERS CREATION FLOWCHART.

SUPERCLUSTERING METHOD

For clusters created using the fixed times method, each cluster is then checked for any overlapping cluster with the time difference of 120 minutes. If so, the clusters are combined into a supercluster. This process is repeated for each cluster until all epochs are checked. The result of this process is the hotspot superclusters.

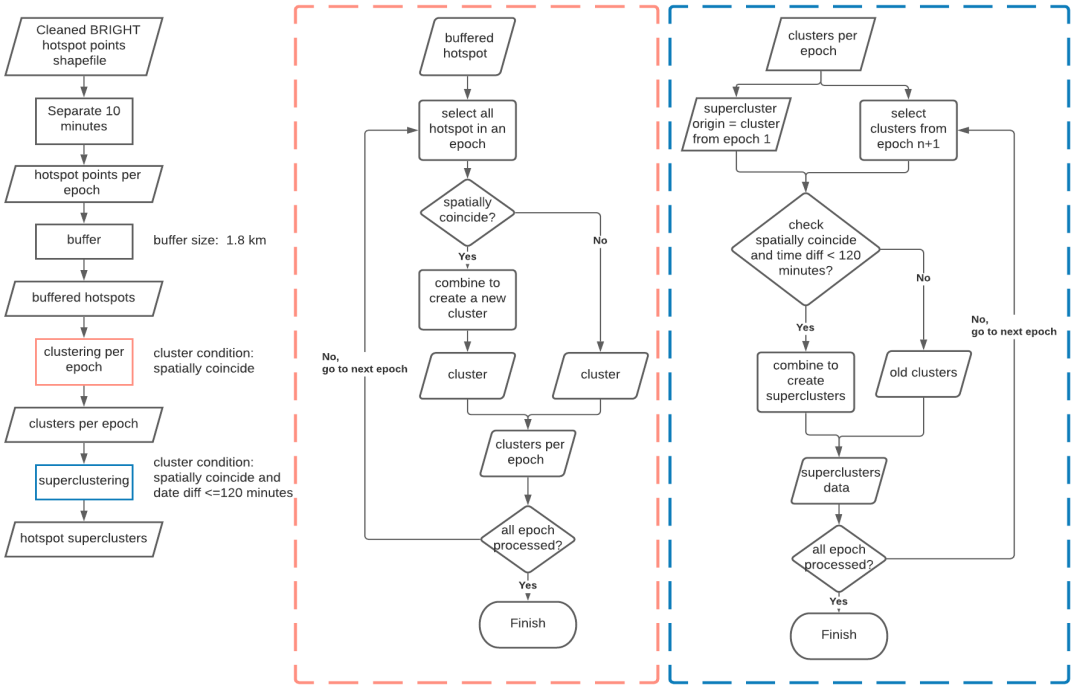

FIGURE 6. HIMAWARI-8 HOTSPOTS SUPERCLUSTERS CREATION FLOWCHART.

SUMMARY OF OUTPUT PRODUCTS

BRIGHT data was used to create four products. These include the original BRIGHT hotspot data generated using the BRIGHT algorithm and BRIGHT hotspot data with additional fields added for spatial, temporal and draft (unverified) fire radiative power (FRP) flags based on Wooster et al. (2003), and cluster identifiers:

1. BRIGHT Himawari-8 Hotspots
2. Cleaned BRIGHT Himawari-8 Hotspots

Two additional data sets were created using the spatio-temporal clustering method outlined by Lizundia-Loiola *et al.* (2020).

3. Fixed times Himawari-8 hotspot clusters
4. Himawari-8 Hotspots Superclusters* (The presence of data gaps can affect the experimental data products and attributes prepared in this work; that is, the identification of superclusters and respective seed points. These are noted throughout the report and in the associated metadata tables.)

The result of the clustering process depends on the buffer size and time threshold. Appendix A outlines the justification for the buffer size selection while Appendix B describes the justification for the chosen time threshold.

REFERENCES

1 Engel, C. B., Jones, S. D. and Reinke, K. (2020) 'A Seasonal-Window Ensemble-Based Thresholding Technique Used to Detect Active Fires in Geostationary Remotely Sensed Data', *IEEE Transactions on Geoscience and Remote Sensing*, pp. 1–10. doi: 10.1109/TGRS.2020.3018455.

2 Engel, C. B., Jones, S. D. and Reinke, K. J (2021) 'Real time detection of daytime and nighttime fire hotspots from geostationary satellites'. Manuscript submitted for review.

3 Giglio, Louis *et al.* (2015) 'MCD64A1 MODIS/Terra+Aqua Burned Area Monthly L3 Global 500m SIN Grid V006'. NASA EOSDIS Land Processes DAAC. doi: 10.5067/MODIS/MCD64A1.006.

4 Giglio, L. (2016) 'MODIS Aqua & Terra 1 km Thermal Anomalies and Fire Locations V006 NRT'. NASA Land Atmosphere Near real-time Capability for EOS Fire Information for Resource Management System. doi: 10.5067/FIRMS/MODIS/MCD14DL.NRT.006.

5 Lizundia-Loiola, J. *et al.* (2020) 'A spatio-temporal active-fire clustering approach for global burned area mapping at 250 m from MODIS data', *Remote Sensing of Environment*, 236, p. 111493. doi: 10.1016/j.rse.2019.111493.

APPENDIX

JUSTIFICATION OF BUFFER SIZE SELECTION

The result of the clustering process can vary depending on the buffer size applied to the hotspot data. Ideally, the buffer size should reflect the pixel size of the image used to derive the hotspot. However, the size of each pixel can vary depending on its geographic location. The buffer needs to be large enough to be able to connect two adjacent hotspots, while still maintaining a good spatial resolution. Practically, the buffer size should be slightly higher than half the maximum distance between two hotspots in the study area. In this study, a buffer size of 1800 m was chosen since the largest distance between two adjacent hotspots in Kangaroo Island was 3577 m (Figure 8).

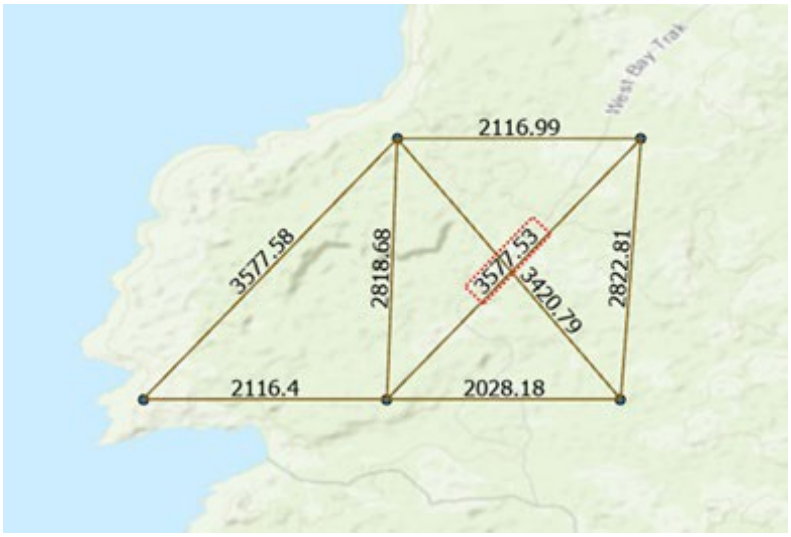

FIGURE 6. HIMAWARI-8 HOTSPOTS SUPERCLUSTERS CREATION FLOWCHART.

JUSTIFICATION OF TIME THRESHOLD SELECTION

Besides the buffer size, the result of the clustering process also depends on the time threshold used in the superclustering process. The time threshold represents the maximum time difference between two overlapping hotspots, so that the hotspots can still be considered a single phenomenon or a cluster. In this study, three time-thresholds (one-hour, two-hour, and three-hour) were chosen and applied to the Kangaroo Island data. Table 3 below shows the statistics of the supercluster product for each time threshold, while Figure 9 and Figure 10 show the histograms of supercluster area and supercluster duration for each time threshold.

Category	**1h**	**2h**	**3h**	**Category**
Number of superclusters	123	80	61	Number of superclusters
Largest supercluster area	1024.3 km^2	1070.9 km^2	1099.1 km^2	Largest supercluster area
Longest supercluster duration	79.8 hrs	102.8 hrs	105.1 hrs	Longest supercluster duration
Mean supercluster area	100.2 km^2	123.4 km^2	135.9 km^2	Mean supercluster area
Mean supercluster duration	4.1 hrs	6.9 hrs	9.5 hrs	Mean supercluster duration

TABLE 3 STATISTICS OF SUPERCLUSTER USING 1 HOUR, 2 HOURS, AND 3 HOURS THRESHOLD.

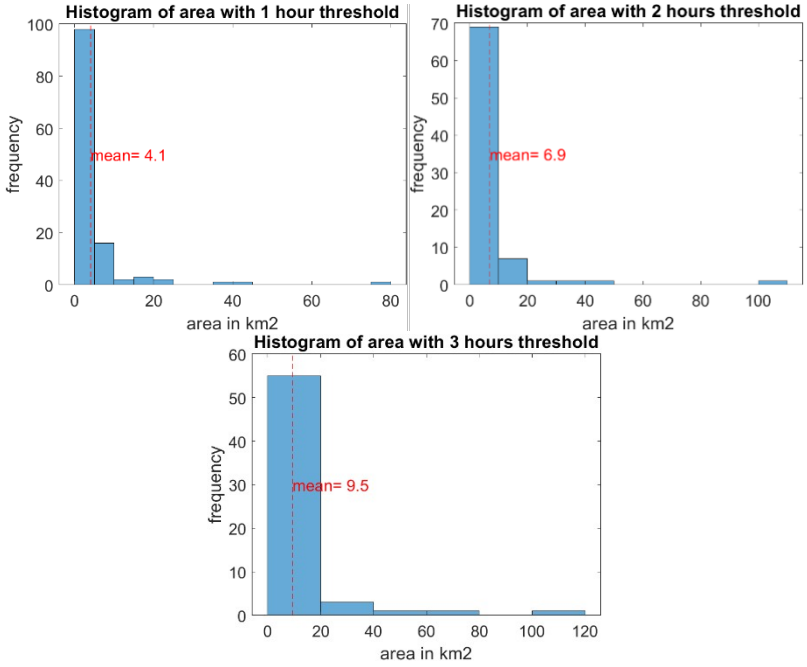

FIGURE 9 FREQUENCY DISTRIBUTION OF SUPERCLUSTERING AREA FROM SUPERCLUSTERING WITH 1 HOUR, 2 HOURS, AND 3 HOURS TIME-THRESHOLD.

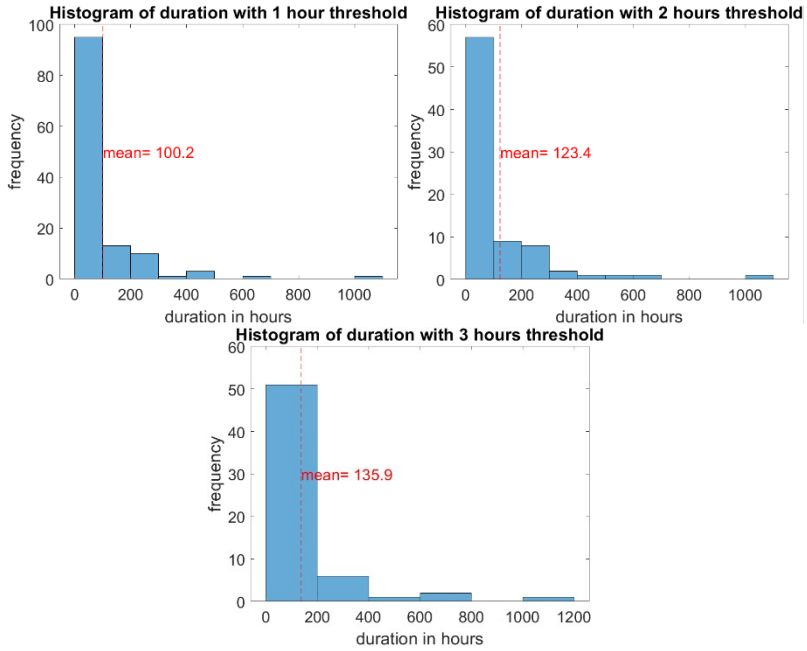

FIGURE 10 FREQUENCY DISTRIBUTION OF SUPERCLUSTERING DURATION FROM SUPERCLUSTERING WITH 1 HOUR, 2 HOURS, AND 3 HOURS TIME-THRESHOLD.

Based on the statistics above, a 2-hour time-threshold was selected because it provides clusters with the best cluster distribution. We expected the 2-hour time-threshold to produce clusters with a good balance between spatial and temporal accuracy. The 1-hour time-threshold was inappropriate because it separates the supercluster with the longest duration and supercluster with the largest area, while the 3-hour time-threshold produces too many clusters of similar duration.